Macromolecules **1998,** *31,* 7791−7799

Structure Evolution of Spherulitic Crystallization in Semicrystalline Polymer Films

Tao Huang, A. D. Rey,* and M. R. Kamal

Department of Chemical Engineering, McGill University, 3610 University Street,
Montreal, Quebec H3A 2B2, Canada

Received January 29, 1998; Revised Manuscript Received August 5, 1998

ABSTRACT: Isothermal nucleation-growth phenomena in 2D semicrystalline polymer films have been investigated by the time-resolved two-dimensional fast Fourier transform (2DFFT) as a quasi-scattering method via real-time in situ observation and measurements. The dynamic evolution of the structure function has been used to interpret the observed scattering intensity connected with crystallization kinetics. The important dynamic quantities, such as the intradomain scattering (domain-size distribution) and spatial distribution of nuclei, have been distinguished by the analysis of the power spectra for different crystallization conditions. The interdomain interference (spatial correlations) was interpreted by the aid of a pair correlation function. Experimental data confirm Porod's law, that is, the q^{-4} dependence of the tails. A scaling relation of the structure function is found experimentally for the free growth of domains during the postnucleation stage; however, it is not valid after impingement occurs.

Introduction

Spherulitic crystallization is a long-standing issue, central to polymer science.[1] On the macroscopic scale, experimental observation shows the spherulites with a spherical envelope and constant growth velocity before impingement under isothermal crystallization conditions.[2] The nucleation-growth process is of great importance in determining crystalline morphology. The number and distribution of the nuclei can profoundly affect the orientation and properties of the material after solidification.[3] However, there have been few studies on the characteristics of the structure evolution, such as the domain-size distribution and spatial distribution of nuclei during the nucleation-growth process, which is the prospective of the present study.

Theoretically, structure evolution during nucleation and growth of crystals from the melt remains one of the most interesting aspects of condensed-matter and materials science.[4] The Kolmogorov−Johnson−Mehl−Avrami (KJMA)[5] theory has been used to analyze experimental data by describing the time dependence for the transformed fraction. Kinetic studies of first-order phase transitions have been devoted to the characterization and evaluation of structure factors and their relationship with time-dependent diffraction studies.[4] Structure evolution was studied theoretically by Sekimoto[6] based on two-point correlation functions, similarly extended by Axe and Yamada[7] and also by Ohta et al.[8] Hermann[9] presented an analytical expression and computational simulation to relate the small-angle scattering intensity to the transformed volume fraction for crystallization kinetics based on a stochastic model. However, there is no experimental validation so far in any material systems.

From an experimental point of view, the time-dependent spatial correlation and structure factor evolution have been extensively used in studying phase-ordering kinetics.[4] Light scattering has been widely used in the polymer field.[10] The polarized light scattering of spherulites in semicrystalline polymers has been extensively studied by Stein and co-workers.[10] Experiments of dynamic light scattering have been carried out in a range from spherulite deformation[11] to spherulite growth.[12] However, the dynamics of nucleation and growth of spherulitic domains has not been systematically studied so far. Experimental results of small-angle scattering in the early stages of nucleation and growth in mixtures of low-molecular-weight compounds, colloidal suspensions, and polymer blends have been recently reported.[13] During the postnucleation stage, the structure evolution has hitherto not been accessible for characterization by light scattering, because the phenomena occur on a micromole to millimole scale. However, two-dimensional Fourier transform operation on a real-space image corresponds to a light scattering experiment.[14] The physical information from each of these two operations is equivalent. The power spectrum of an image is equivalent to that obtained by small-angle light scattering in certain cases, for example, phase separation.[14]

In order to investigate postnucleation and growth phenomena in 2D semicrystalline polymer films, a direct imaging technique of time-resolved two-dimensional fast Fourier transform (2DFFT) has been used via real-time in situ observation and measurements. In this paper, we present the basic principles of image modeling and the technical procedures of calibration, interpretation, and power spectrum estimation of 2DFFT of images of the dynamic structure factors and form factors. Dynamic evolution of the structure function has been used to interpret the observed scattering intensity connected with crystallization kinetics. It is discussed in relation to the experimental results obtained from the time-resolved 2DFFT operation by digital image analysis applied to polymer spherulitic crystallization. The important dynamic quantities, such as the intradomain scattering (domain-size distribution), spatial distribution of nuclei, and transformed volume fraction, have been distinguished by the analysis of the power spectrums for different crystallization conditions. The interdomain scattering (spatial correlations) has been interpreted with the aid of a pair correlation function. A scaling relation of the structure function has been evaluated with the experimental data for multiple spherulitic growth during the postnucleation stage.

---

* To whom correspondence should be addressed.

10.1021/ma9801218 CCC: $15.00

Experimental Methods

Experimental Procedures. Experiments were carried out with isotatic polypropylene (iPP; molecular weight $M_\eta = 250\,000$). A thin polymer film was formed between two glass slides, while pressing the top slide to form a 10-μm thick polymer film. In this study, we focused on the postnucleation stage. The size of the nuclei was greater than 1 μm and visible under the optical microscope for real-time in situ observation and accurate real-space measurement. Due to the slow dynamics of polymer crystallization, deeper quench or larger supercooling ($\Delta T = T_m - T_c \gg 1-10$ °C) was needed for normal nucleation and growth, so that the small thermal fluctuations had less effect on the system.

The time-resolved video microscope system consisted of a Zeiss microscope, a CCD video camera, a videotape recorder, and a computer image acquiring and processing system. The microscope had sufficient magnification objectives (40×, 10×, 4×, and 2.5×) to study morphologies of the postnucleation and growth from micrometer structures to structures on the order of several millimeters. A CCD video camera, with 256-Gy levels, was mounted on the microscope, enabling us to view the image on a monitor. During an experiment, we recorded the images on a Sony videocassette recorder to facilitate examination of the data. The camera and the digitization processor were tested in order to check the linearity in intensity and also the homogeneity of the pattern.

Measurement of the Power Spectrum. For polymer spherulitic crystallization, the nucleation and growth is a first-order phase transition. The order parameter is the semicrystalline spherulite, thus

$$\psi(\vec{\mathbf{r}},t) = \begin{cases} 1 & \text{if } \vec{\mathbf{r}} \in \text{spherulitic domain at time } t \\ 0 & \text{if } \vec{\mathbf{r}} \ni \text{spherulitic domain at time t} \end{cases} \tag{1}$$

According to eq 1, the order parameter is 1 in a spherulite and 0 in the melt. Relying on this assumption, all the texture within spherulites was removed, and the gray scale images were converted to binary images to perform the FFT operation.

The principle of obtaining 2DFFT power spectrum from an image was given by Tanaka et al.[14] The principles of light scattering, data treatment, and interpretation of the scattering spectrum are given in the literature.[15] We performed a 2DFFT of the digitized intensity of the real-space binary image and computed the square of its modulus $I(q_i,t)$, where i is an index running from 1 to 512 × 512, which denotes each pixel. In power spectrum estimation and interpolation, a high-quality noise-free image was preferred. Before doing 2DFFT transform, usually a correction for the inhomogeneous distribution of light intensity was necessary in order to obtain a highly homogeneous image to minimize the so-called leakage effect. Surface fitting can be used for noise removal when one of the noise components can be fitted, computed, and subtracted out. This can be achieved by fitting a background surface to the intensity profile of the image or a portion thereof, by using a two-dimensional polynomial or Guassian function.

As in light scattering, there was a central spot on the spectrum image due to the light beam passing directly through the sample without scattering. In data analysis, we removed the central spike and set as the average value of its neighbors. Then, we performed the azimuthal averaging to get the power spectrum plot $I(q)$ vs q, if radial symmetry was observed. We calibrated q by using the microscopic image of a scale. We did not calibrate the I axis, since we were not interested in the absolute intensity. In this study, we kept the incident light of the microscope constant during the whole experimental run.

Interpretation. To probe the information of the spatiotemporal evolution from the FFT power spectrum, we propose that the structure evolution is proportional to the observed power spectrum of the scattered intensity $I(\vec{\mathbf{q}})$. Basically, the observed scattered intensity is dominated by

$$I(\vec{\mathbf{q}}) = B(\vec{\mathbf{q}}) + P_m(\vec{\mathbf{q}})S_m(\vec{\mathbf{q}}) + N_s P(\vec{\mathbf{q}})S(\vec{\mathbf{q}}) \tag{2}$$

where $B(\vec{\mathbf{q}})$ is the background contribution, $P_m(\vec{\mathbf{q}})$ and $P(\vec{\mathbf{q}})$ are observed form factors of the melt and solid spherulitic growth domain, respectively, $S_m(\vec{\mathbf{q}})$ and $S(\vec{\mathbf{q}})$ are observed structure factors of the melt and solid spherulitic growth domain, respectively, and N_s is the total number of spherulitic growth domains.

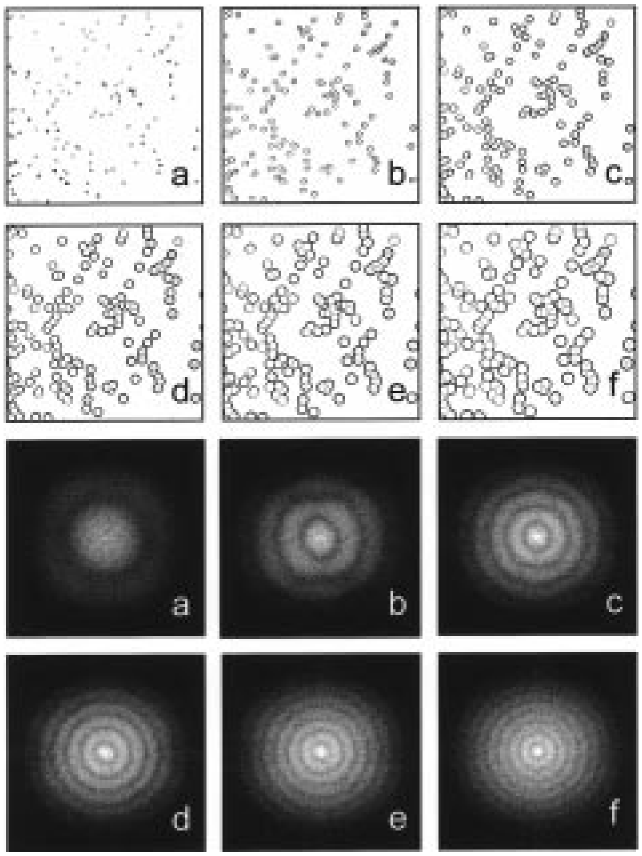

Figure 1. Pattern evolution of iPP spherulite nucleation growth in real space and in Fourier space for a simultaneous nucleation case under isothermal conditions, $T_c = 129.0$ °C. The size of all real-space images is 2521 × 2521 μm. The times for the images are (a) 300, (b) 900, (c) 1800, (d) 2700, (e) 3600, (f) 4500 s.

The background contribution during nucleation and growth can be assumed to remain constant, because we kept the incident light of the microscope constant during the whole experimental run. The second term in eq 2 is the result of the interparticle interference from the microdomains of supermacromolecular structures in the polymer melt. This is not accessible for characterization from the light microscope image. The third term represents spherulite scattering and shows up as a series of peaks in the scattered spectrum.

Therefore, under the experimental conditions, the scattering intensity can be defined as:

$$I(\vec{\mathbf{q}}) \propto N_s P(\vec{\mathbf{q}})S(\vec{\mathbf{q}}) \tag{3}$$

It depends on both the particle spatial correlations, called structure factor $S(\vec{\mathbf{q}})$, and the particle size distribution, called form factor $P(\vec{\mathbf{q}})$. In principle, information on the structure factor can be obtained by examining the small wavenumber behavior of the structure function. However, it is very difficult to determine the structure factor from the observed scattering spectrum, because the size distribution suppresses the oscillations of the structure factor. Thus, it is analyzed with the aid of an inverse calculation from a pair correlation function.

Experimental Results

The images in Figures 1−3 show the experimental results of the real-space snapshots and the corresponding 2DFFT power spectrum, taken at different times for

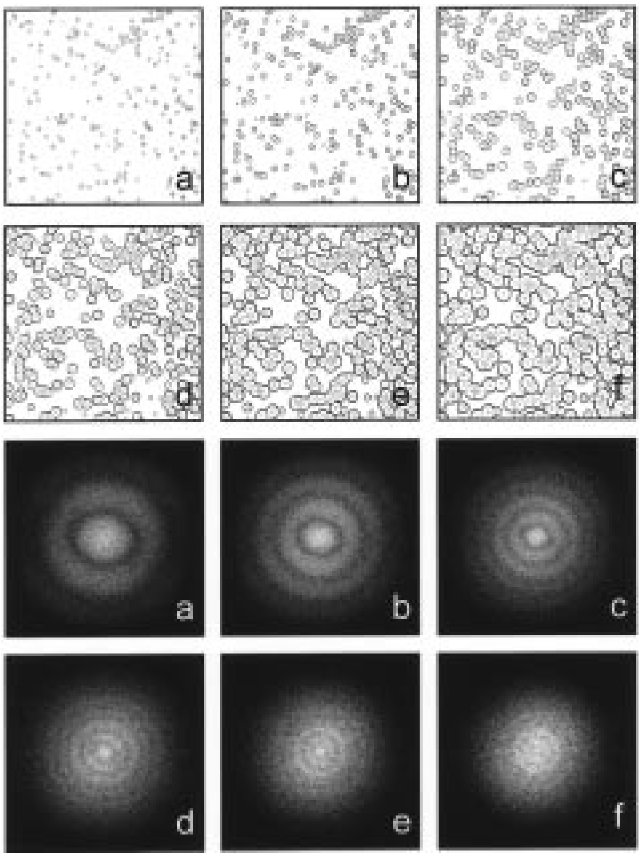

Figure 2. Pattern evolution of iPP spherulite nucleation growth in real space and in Fourier space for a continuous nucleation case under isothermal conditions, $T_c = 133.0$ °C. The size of all real space images is 2521 × 2521 μm. The times for the images are (a) 300, (b) 1200, (c) 3000, (d) 3900, (e) 4800, (f) 5700 s.

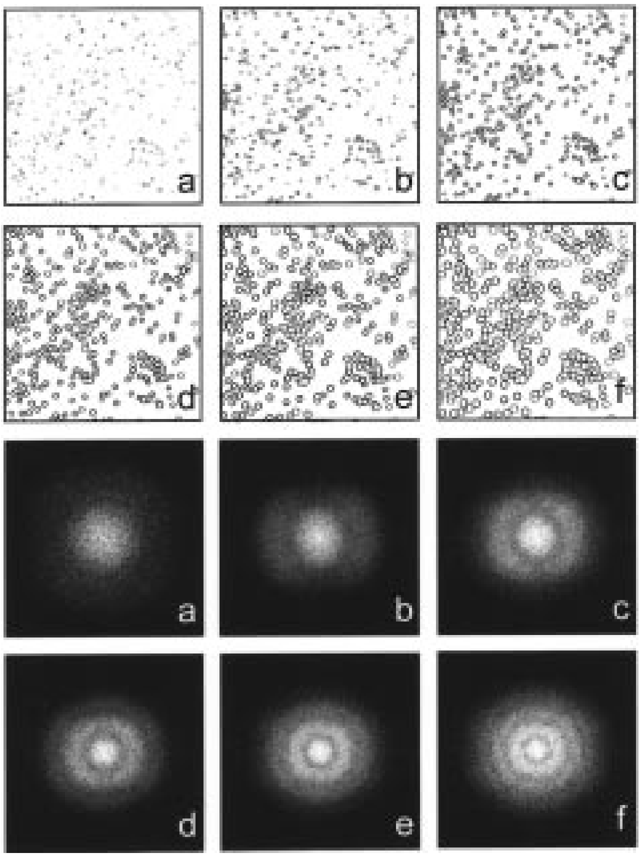

Figure 3. Pattern evolution of iPP spherulite nucleation growth in real space and in Fourier space for a continuous nucleation case under isothermal conditions, $T_c = 135.0$ °C. The size of all real space images is 2521 × 2521 μm. The times for the images are (a) 600, (b) 3600, (c) 7200, (d) 10 800, (e) 14 400, (f) 18 000 s.

three different isothermal nucleation and growth processes. All of the real-space images in Figures 1−3 are gray scale images in order to show a clear view of the processes. The 2DFFT operation was performed on binary images which were converted from the corresponding gray scale images.

In Figure 1, the real-space images show the pattern evolution of simultaneous nucleation and constant growth at $T_c = 129.0$ °C. The number of nuclei is constant with time, and they grow in size at a constant velocity before impingement. The isolated spherulites grow radially with constant velocity, 0.035 μm/s, before impingement. This means that the spatial correlation of the center of a spherulite domain is time-independent and that only the characteristic size of a spherulite grows linearly with time until impingement occurs. In Fourier space, the radii of the scattering rings decrease with increasing time. Importantly, the rings of the scattered light exhibit an almost periodic feature in the peak positions before, and even after, impingement for some time, while the transformed fraction is smaller than 0.5. This means that there is one characteristic length changing with time in the system.

Figure 2 shows the real-space snapshots and the corresponding 2DFFT images of the spatio-temporal evolution of nucleation and growth in continuous nucleation under isothermal temperature $T_c = 133$ °C. The isolated spherulites grow radially with constant velocity, 0.02326 μm/s, before impingement. Although the images in Figure 2 are focused on the domain growth in postnucleation stage, they show that there is a size distribution of the spherulite domains. There are still some new nuclei appearing in each of the real-space images shown in Figure 2a−c. Experimental observation shows that the initial nucleation rate could be very high but that it soon decays to the linear steady-state value for a short time, and then it gradually decays to zero. During the early growth stage, experimental measurements show that the mean distance to the next nucleus decreases with increasing time. The size of the depletion zone surrounding each nucleus also decreases with time. The mean distance to the next nucleus is more distinct at higher area fractions, with nuclei packing more densely. The partial pair correlation function for new nuclei to old nuclei shows that the new nuclei tend to appear randomly near old nuclei.[17]

Figure 3 shows another set of the real-space snapshots and the corresponding 2DFFT images of the spatio-temporal evolution of nucleation and growth in continuous nucleation under isothermal temperature $T_c = 135$ °C. The isolated spherulites grow radially with constant velocity, 0.018 μm/s, before impingement. The elliptic shape of the scattering rings in FFT images a, b, and c, in Figures 2 and 3 is due to clustering of nuclei. It disappears at later stages, because the overlapping of the impinged domains becomes large. Compared to Figure 1, the rings of the scattered light of 2DFFT images in Figures 2 and 3 are less distinct and without periodic features. The rings in Figure 3 are more coarse than those in Figure 2, which reflects a higher nucleation density and clustering. The experimental results show that the rings become smaller in size and brighter

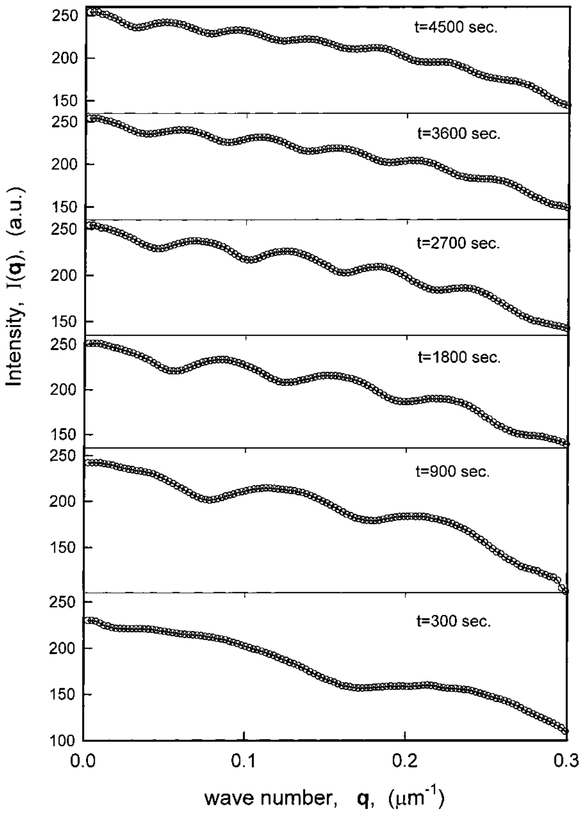

Figure 4. Experimental results of the scattering intensities from FFT for a simultaneous nucleation case under isothermal conditions, $T_c = 129.0$ °C.

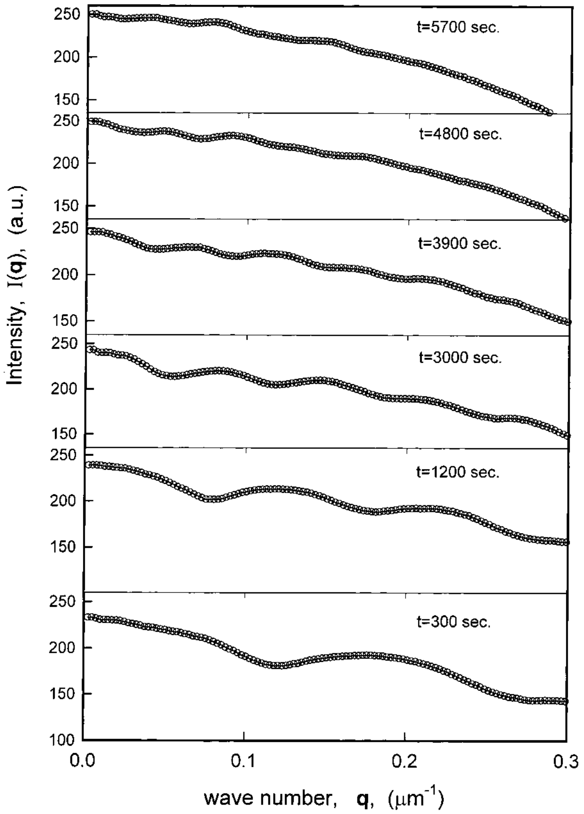

Figure 5. Experimental results of the scattering intensities from FFT for a continuous nucleation case under isothermal conditions, $T_c = 133.0$ °C.

in intensity as a function of time. This behavior reflects both an increase in nucleation density and the growth of the domains.

Figure 4 shows the results for the dynamic structure functions from the FFT for the simultaneous nucleation case under isothermal conditions $T_c = 129.0$ °C. Figure 5 shows the results for the dynamic structure functions from FFT for the continuous nucleation case at $T_c = 133.0$ °C. Figure 6 shows the results for the dynamic structure functions from FFT for the continuous nucleation case at $T_c = 135.0$ °C. The peaks at high q values are mainly due to intraspherulite scattering, which represents the size distribution of the spherulitic growth domains. Figure 4 shows that the high q peaks in the simultaneous nucleation case are more distinct with relatively higher amplitudes, when compared to Figures 5 and 6 in the continuous nucleation cases.

Discussion

Experimental results show that there are a number of scattering maxima on each scattering curve. There is a weak peak with small q_s value on the scattering central shoulder, which is assumed to be the interference peak representing the spatial correlation of the nuclei, the structure factor $S(q)$. A number of broad scattering maxima may be considered to be first- and higher-order scattering maxima. However, the maximum scattering intensity is located at $q_m = 0$. In details, Figure 7 shows the structure analysis results of the scattering intensity. The inserted images show the real-space image and corresponding FFT image. In Figure 7, there is a weak peak with a small $q_s = 0.0251$ μm value on the scattering curve, which is indicated by a thick arrow. The detail is shown in an inserted zoom plot in Figure 7. This is considered to be the interference peak representing the spatial correlation, namely, the structure factor $S(q)$. The high q peaks, q_1, q_2, q_3,..., represent the form factors due to the major contribution of intraspherulite scattering, which represent the size distribution of the particles. The scattering q's are clearly identified in Figure 7.

In the next section, we discuss the characteristic of the intradomain scattering, interdomain scattering, and analysis of the spatial distribution of nuclei from the scattering curves. For further dynamic studies, we discuss the validation of Porod's law,[16] which applies for scattering from a material which has a sharp interface between alternating regions of two distinct densities. The scaling relation for nucleation growth is evaluated from experimental data.

Intradomain Scattering: Domain-Size Distribution. During the free growth stage, the transformed volume fraction is $\phi \ll 0.5$. The isothermal nucleation and growth can be treated as a monodisperse droplet system, for the simultaneous nucleation case, and a polydisperse droplet system, for the continuous nucleation case. For the continuous nucleation case, the following expression can be used to calculate the average necessary for computing the scattering:

$$\langle |\mathrm{F}(\vec{\mathbf{q}})|^2 \rangle = \int_0^\infty |F(q,R)|^2 \, f(R) \, \mathrm{d}R \tag{4}$$

$$|\langle F(\vec{\mathbf{q}}) \rangle|^2 = |\int_0^\infty F(q,R) \, f(R) \, \mathrm{d}R|^2 \tag{5}$$

where $F(q,R)$ is the form factor for a spherulite of radius R, which is connected with Guinier approximation[15]

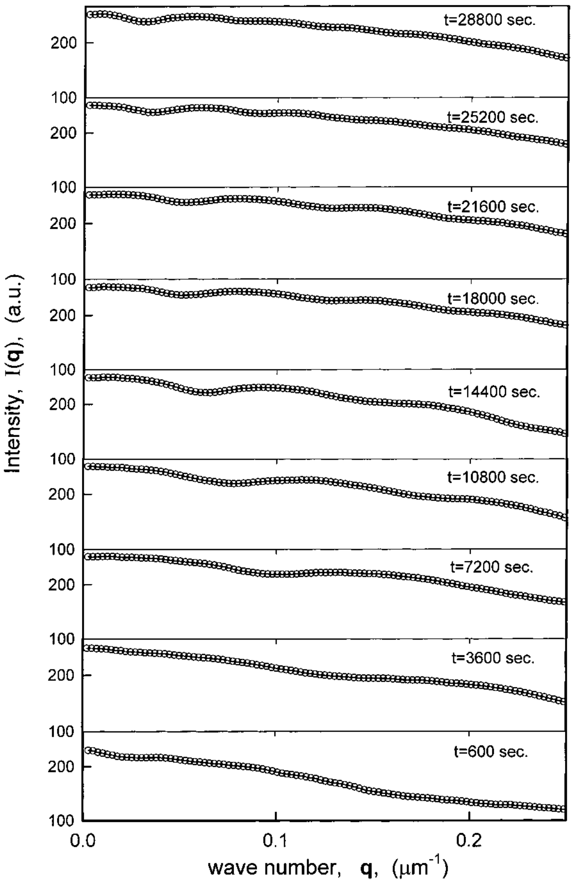

Figure 6. Experimental results of the scattering intensities from FFT for a continuous nucleation case under isothermal conditions, $T_c = 135.0$ °C.

$$F(q,R) = \left[3\frac{qR\cos(qR) - \sin(qR)}{(qR)^3}\right]^2 \tag{6}$$

and $f(R)$ is the probability of a domain having a size between R and $R + dR$, where R is the spherulite radius. The expression of $f(R)$ is dependent on the nucleation kinetics, which is different for different experimental conditions.

The form factor $P(\vec{q})$ can be expressed as:

$$P(\vec{q}) = \langle |F(\vec{q})|^2 \rangle \tag{7}$$

The size distribution, $f(R)$, can be fitted by suitable probability functions to experimental data, which could be different and dependent on the experimental conditions. Figure 8 shows the fitting result of eq 7 for the experimental data in Figure 7. The absolute value of the scattering intensity is meaningless because it was not calibrated. However, the positions of the first- and higher-order scattering maxima agree with experimental data very well. This result shows that the application of droplet scattering for nucleation growth before impingement works very well.

Interdomain Interference: Spatial Correlation. The structure factor $S(\vec{q})$ in eq 3 can be expressed using Kotlarchyk and Chen's results,[18] as follows:

$$S(\vec{q}) = 1 + \beta(\vec{q})[S'(\vec{q}) - 1] \tag{8}$$

$$\beta(\vec{q}) = |\langle F(\vec{q})\rangle|^2 / \langle |F(\vec{q})|^2 \rangle \tag{9}$$

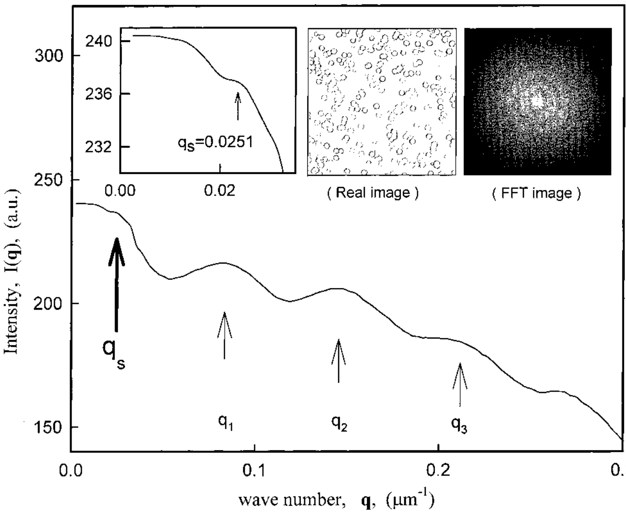

Figure 7. Typical structure analysis result of the scattering intensity. The inserted images show the real-space image and corresponding FFT image. There is a weak peak with a small $q_s = 0.0251$ μm value on the scattering curve, which is indicated by a thick arrow. The detail is shown in an inserted zoom plot. It is supposed to be the interference peak representing the spatial correlation, namely, the structure factor $S(q)$. The high q peaks, q_1, q_2, q_3,..., represent the form factors due to the major contribution of intraspherulite scattering, which represent the size distribution of the particles.

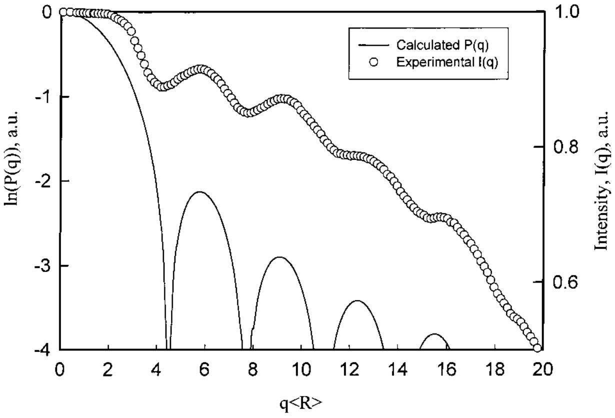

Figure 8. Fitting result of the form factor for Figure 7. The absolute value of the scattering intensity is meaningless because it was not calibrated. The positions of the first- and higher-order scattering maxima agree with experimental data.

where $S(\vec{q})$ acts as an apparent internuclei structure factor and $\beta(\vec{q})$ is a $\vec{q}$-dependent factor between 0 and 1 that suppresses the oscillations of the true structure factor $S'(\vec{q})$ in the observed scattering spectrum from a polydisperse or nonspherical system. Therefore, eq 3 can be expressed as:

$$I(\vec{q}) \propto N_s P(\vec{q})[1 + \beta(\vec{q})[S'(\vec{q}) - 1]] \tag{10}$$

The information on the pure structure factor can be obtained by examining the small wavenumber behavior of the structure function. It can be analyzed with the aid of the inverse analysis of the pair correlation function. The pure structure factor can be calculated by using the pair correlation function, $g(r)$. The function of $g(r)$ is defined as the probability of finding another particle as a function of distance from the center of a particular particle, r, statistically averaged over the system. The structure factor, $S'(q)$, and the pair correlation function, $g(r)$, are related by the following Fourier transform equation:

$$S'(q) = 1 + 4\pi\bar{\rho}\int_0^{\infty}[g(r) - 1]\,\frac{\mathrm{in}(qr)}{qr}r^2\,\mathrm{d}r \qquad (11)$$

where $\bar{\rho}$ is the number density. Figure 9 shows the calculated results of the pair correlation function, $g(r)$, and the corresponding structure factor, $S'(q)$, for the experimental case in Figure 7. In Figure 9, the shapes of the calculated $S'(q)$ in the wave vector domain and $g(r)$ in real space are remarkably similar. For the pair correlation function, $g(r)$, there are smooth peaks that asymptotically approach 1, confirming the complete absence of long-range order. The first maximum peak, $r = 368\ \mu$m, defines the mean distance to the next nucleus. The pronounced first peak shows that the shell of nearest-neighbor nuclei is well-defined. For the structure factor, $S'(q)$, the first sharp peak reflects the existence of a dominant, nearly regular arrangement of the nuclei in real space. The position of the main peak of $S'(q)$ is $q_m = 2\pi/\lambda_m = 0.0259\ \mu\mathrm{m}^{-1}$, in good agreement with the period ($\lambda_m = 242.5\ \mu$m) of the oscillations of $g(r)$ and also with the experimental data $q_s = 0.0251\ \mu$m. The sharp decrease of $g(r)$ at small separations is responsible for the subsequent maxima and minima of $S'(q)$, which become more and more damped as q increases. At large wave vectors, $S'(q)$ probes the "hard core" region where $g(r)$ is vanishingly small and $S'(q) \to 1$. $S'(q) \to 0$ reflects, in an average sense, the features of $g(r)$, including its asymptotic approach to 1 at very large r. The same analysis is valid for all experimental runs.

Pattern Evolution. According to the above analysis, the scattering intensity of the nucleation-growth patterns can be explained by the following equation, which is the combination of eqs 6, 10, and 11.

$$\begin{aligned} I(q) &\propto N_s\int_0^{\infty}|F(q,R)|^2 f(R)\,\mathrm{d}R[1 + \beta(q)[S'(q) - 1]] \\ &= N_s\int_0^{\infty}\left[3\frac{qR\cos(qR) - \sin(qR)}{(qR)^3}\right]^2 f(R)\,\mathrm{d}R \times \\ &\qquad \left[1 + 4\pi\bar{\rho}\beta(q)\int_0^{\infty}[g(r) - 1]\,\frac{\sin(qr)}{qr}r^2\,\mathrm{d}r\right] \end{aligned} \qquad (12)$$

This equation clearly indicates that the observed scattering spectra of the nucleation-growth patterns before impingement are mainly due to polydisperse droplet scattering. The contribution of the structure factor, in the observed scattering spectrum, was suppressed by the polydisperse size distribution, which is expressed by a factor $0 < \beta(q) < 1$.

When impingement occurs, the droplet picture is no longer correct. In the impingement stage with small transformed volume fraction ($\phi < 0.5$), the spherulitic growth domains consist of the polydisperse isolated circular domains and some connected polygon grains. With large transformed volume fraction, the growth patterns are the islands of grain structures and the contribution of impingement becomes important. Grain boundary scattering will dominate the later stages.

Spatial Distribution of Nuclei. The structure factor reflects the characteristics of the spatial correlation. Alternatively, the details of the nuclei distribution in the space and the features of the nuclei densities are also captured by the scattering curves. This can be interpreted by a stochastic model for scattering data.[9] In the stochastic model, the scattering intensity is described by the density−density correlation function of a random set of points, which is given by:

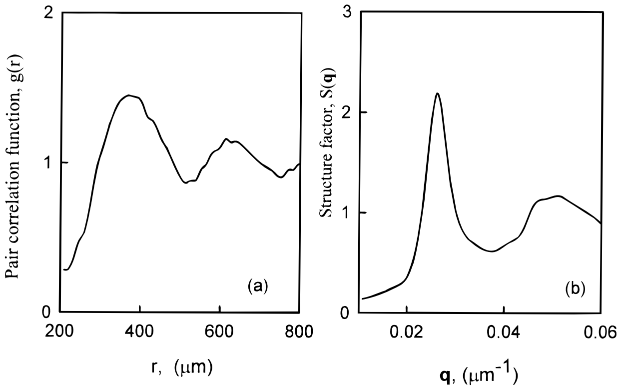

Figure 9. Calculated pair correlation function (a) and corresponding structure factor (b) for Figure 7. The position of the main peak of $S'(q)$ is $q_m = 2\pi/\lambda_m = 0.0259\ \mu\mathrm{m}^{-1}$, in good agreement with the period ($\lambda_m = 242.5\ \mu$m) of the oscillations of $g(r)$ and also with the experimental data $q_s = 0.0251\ \mu$m.

$$I(q,t) = 4\pi\int_0^{\infty} r^2[C(r,t) - \chi^2(t)]\,\frac{\sin(qr)}{qr}\,\mathrm{d}r \qquad (13)$$

where $C(r,t)$ is the probability that two random points separated by distance r lie in the growth domain and $\chi(t)$ is the transformed fraction. In two-dimensional case, $\chi(t)$ is defined as $\chi(t) = 1 - \exp[-\lambda I V^2 t^3]$, where λ is the number density, t is time, and I and V are the nucleation rate and growth velocity, respectively. If $C(r,t) \to 0$, the nuclei are widely spaced and act Poisson-distributed. If $0 < C(r,t) < 1$, the nuclei are distributed uniformly and the probability of the overlapping of grains increases with $C(r,t)$. If $1 < C(r,t) < 2$, the nuclei are of cluster point field with increased nucleation probability in certain regions. For $C(r,t) \gg 1$, the clusters lose their cluster-like nature.

In Figure 4, the curves exhibit significant first-order maxima for low-volume fractions. The peaks are characteristic for a hard-core model with nonoverlapping droplets.[9] With increasing volume fraction, this peak disappears as the structure of the system is now far different from the structure of the generating nuclei and the overlapping of the grains becomes larger. Figure 6 shows the data for the patterns in Figure 3, which have high nuclei density and clustering in nuclei distribution. In Figure 6, at low-volume fractions no sharp peaks are present. With increasing volume fraction, the amplitude of the oscillations first increases and then decreases again.

For the lower transformed fraction, Figure 10 shows a detailed comparison concerning the differences in the nuclei spatio-temporal distribution for three isothermal cases, at the same transformed fraction, $\chi = 0.3$. Figure 10a is for the simultaneous nucleation case in Figure 1, Figure 10b for the continuous nucleation case in Figure 2, and Figure 10c for the continuous nucleation case in Figure 3 with high nuclei density and the clustering in nuclei distribution. In Figure 10a, the first- and high-order maxima are well-defined. In Figure 10b, the amplitudes of the high-order maxima are damped in comparison to Figure 10a. This suppression is more significant, due to the high nuclei density and the clustering in Figure 10c. Therefore, the experimental results show that it is fairly easy to

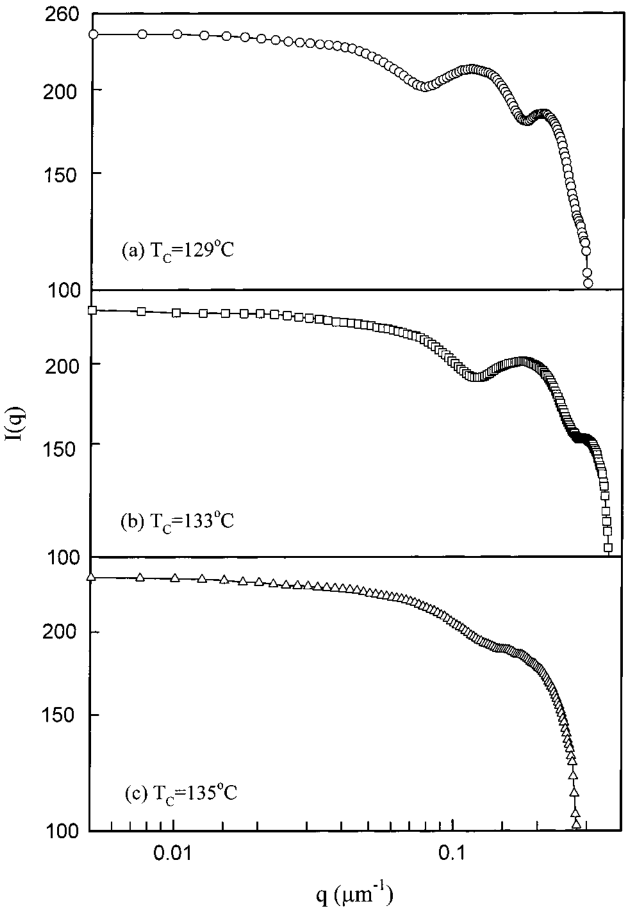

Figure 10. Detailed comparison considering the differences in the nuclei spatio-temporal distribution with the same transformed fraction, $\chi = 0.3$: (a) for the simultaneous nucleation case in Figure 1, (b) for the continuous nucleation case in Figure 2, and (c) for the continuous nucleation case in Figure 3.

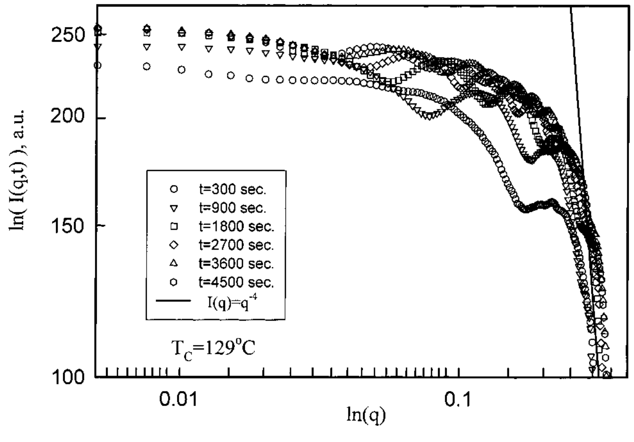

Figure 11. Experimental results of the overall crystallization kinetics from FFT under isothermal conditions for a simultaneous nucleation case at $T_c = 129.0$ °C. The final slope of the structure function is in proportion to q^{-4}.

distinguish the differences between the nucleation kinetics and nuclei distributions from the scattering curves, when the transformed fraction is low.

Porod's Law. Figures 11−13present the scattering intensity, given as a plot of $\ln(I(q,t))$ as a function of $\ln(q)$, which correspond to Figures 1−3, respectively. Experimental data show the q^{-4} dependence of the final slope of the scattering curves, which corresponds to Porod's law.[15] In a crystallization case, Porod's law can be derived from Sekimoto's model.[6] We obtain the scattering intensity for $(\pi IV^2t^3)/3 \ll 1$ in the 2D case as:[19]

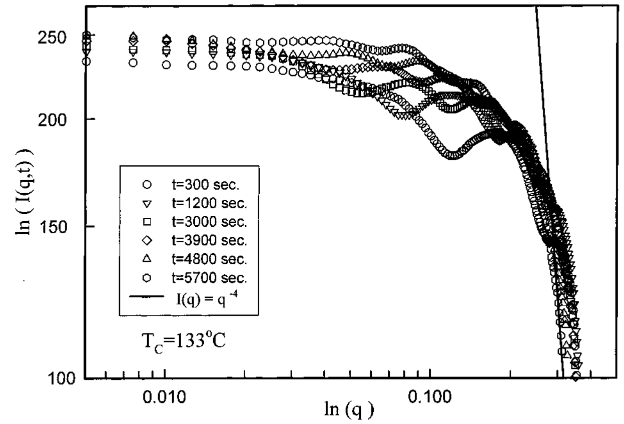

Figure 12. Experimental results of isothermal crystallization of isotatic polypropylene film from FFT for a continuous nucleation case at $T_c = 133.0$ °C. The final slope of the structure function is in proportion to q^{-4}.

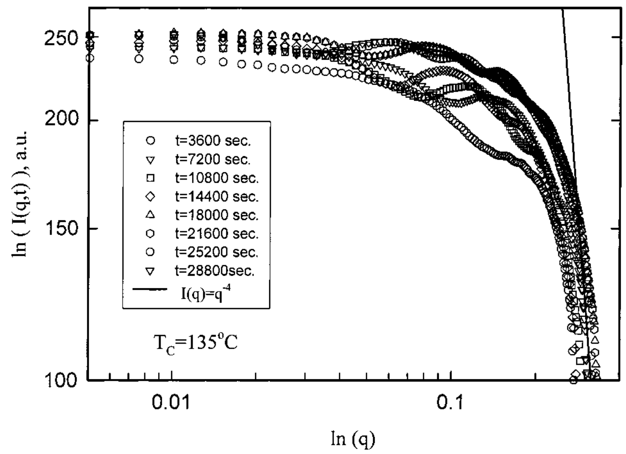

Figure 13. Experimental results of the overall crystallization kinetics from FFT under isothermal conditions for a continuous nucleation at $T_c = 135.0$ °C. The final slope of the structure function is in proportion to q^{-4}.

$$I(q,t) \cong \frac{8\pi^2}{3}\frac{IVt^2}{q^4}\exp\left(-\frac{2\pi}{3}IV^2t^3\right) \qquad (14)$$

This suggests that the final slope of the structure function is proportional to q^{-4} since the real-space structure contains a well-defined interface between the spherulitic growth domains.

Scaling Relation. The scaling relation for structure factor is an important phenomenon in condensed-matter physics.[4] The basic idea underlying the scaling is that after some initial transient time following a quench, a characteristic, time-dependent length scale, $q_m(t)$, is established. The scaling hypothesis states that there exists, at late times, a single characteristic length, $-1(t)$, such that the domain structure is, in a statistical sense, independent of the time when lengths are scaled by $q_m(t)$.

For systems in which the order parameter is conserved, such as the late stages of spinodal decomposition, the structure develops by domain merge and growth, in a way which is statistically self-similar in time, apart from a global change of scale. In other words, the average domain size grows and the number

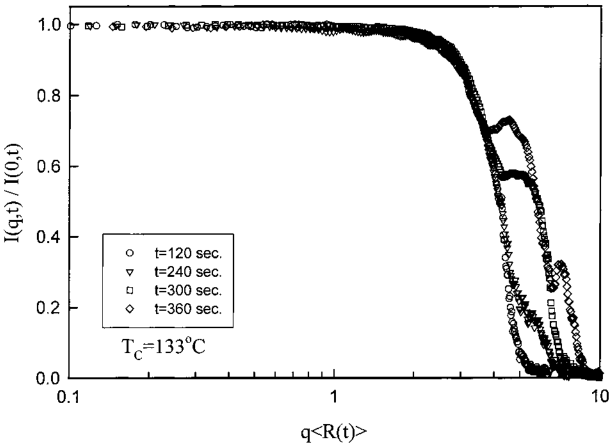

Figure 14. Experimental results of scaling relation at early free growth stage before impingement from FFT for a continuous nucleation case under isothermal conditions $T_c = 133.0$ °C. The scaling is the system dynamic behavior and demonstrates that the spherulitic domains grow in size linearly with time. The scaling is valid for times long enough that the influence of the initial conditions has decayed; the nucleation event is not dominant.

of domains decreases. With a magnification adjusted to scale the domains to have the same average size, the pictures show the same qualitative features. This means that the interparticle distance is proportional to the particle size; therefore, there exits only one relevant length scale, $q_m(t)$, which is well-defined in scattering patterns. The scaling function can be written as $F(q(t)/q_m(t)) = I(q,t)/I(q_m,t)$, and the data for different times will be superposed on one curve.

For the nucleation-growth system, the order parameter is not conserved. Because the amount of solid changes from 0 to 1 during the transformation. The scaling is not theoretically well-understood, due to the system complexity, or experimentally well-characterized, due to the technical difficulties. However, in some related nonconserved systems, e.g., antiferromagnets[20] and phase-ordering processes,[21] the scaling is presumably valid for times long enough that the influence of the initial conditions has decayed.

During the early free growth stage before impingement, the scaling function, $F(q(t)/q_m(t)) = I(q,t)/I(q_m,t)$, cannot be defined in this case because $q_m = 0$. However, by assuming polydisperse spherulitic domains and no interference between the spherulitic domains before impingement, the corresponding scattering intensities can be computed by considering the size distribution. The spherulitic growth domain can be treated as isolated circular domains in the early free growth stage before impingement. The probability $p(R)\,dR$ that a spherulitic domain has a radius between R and $R + dR$ is given by $p(R) = f(R/\langle R(t)\rangle)/\langle R(t)\rangle$, where $\langle R(t)\rangle$ is the time-dependent average radius and $f(R/\langle R(t)\rangle)$ is the size distribution function. We propose to use the Lifshitz–Slyozov function[22] to capture the scaling relation, which is given by:

$$F_{LS}(q\langle R\rangle) = \frac{S(q\langle R\rangle(t),t)}{S(0,t)} \qquad (15)$$

where $\langle R\rangle$ is the average radius of the growth domain.

Figure 14 shows the experimental results of the scaling functions $F_{LS}(q\langle R\rangle)$. In this graph, the maximum of $F_{LS}(q\langle R\rangle)$ is located at $q\langle R\rangle = 0$. Some shoulders appear at large $q\langle R\rangle$, which are the remains of the maxima of the distribution function, slightly smoothed by the averaging over $p(R)$. In fact, these shoulders correspond to oscillations around the average decrease $(q\langle R\rangle)^{-4}$. Finally, the oscillations will disappear completely, leaving only the $(q\langle R\rangle)^{-4}$ decay.

To make clearer the physical picture of nucleation growth, we propose to describe the nucleation-growth process as consisting of three stages. (1) The early structure transition-nucleation stage: A dynamic structure transition occurs, which is related to a change in the thermal fluctuations of the electron density, i.e., to isothermal compressibility.[23] In polymer systems, the trans-zig-zag chain segments are generated at first from the molten random coils, and then these trans segments gather together to form small crystalline clusters, which grow into larger lamellae, as detected by the small-angle X-ray scattering measurements.[24] (2) The postnucleation and early free growth stage: The scaling is the system dynamic behavior and demonstrates that the spherulitic domains grow in size linearly with time. The scaling is valid for times long enough that the influence of the initial conditions has decayed; i.e., the nucleation event is not dominant. This agrees with the recent theoretical results by Monte Carlo simulation[7] and by domain-spatial correlation function.[25] (3) The impingement stage: The scaling will break down because some impinged spherulitic domain clusters become time-independent.

Conclusion

Isothermal nucleation-growth phenomena in 2D semicrystalline polymer films were investigated by the time-resolved two-dimensional fast Fourier transform (2DFFT), as a quasi-scattering method, via real-time in situ observation and measurements. The dynamic evolution of the structure function was used to interpret the observed scattering intensity connected with crystallization kinetics. The important dynamic quantities, such as the intradomain scattering (domain-size distribution) and spatial distribution of nuclei, were distinguished by the analysis of the power spectrum for different crystallization conditions. The interdomain interference (spatial correlations) was interpreted with the aid of a pair correlation function.

Experimental data indicate that the observed scattering spectrum of the nucleation-growth patterns before impingement results mainly from polydisperse droplet scattering. The contribution of the structure factor from the observed scattering spectrum is suppressed by the polydisperse size distribution, which is expressed by a factor $0 < \beta(q) < 1$. When impingement occurs, the droplet picture is no longer correct. In the impingement stage with a small transformed volume fraction ($\phi < 0.5$), the spherulitic growth domains consist of the polydisperse isolated circular domains and some connected polygon grains. With a large transformed volume fraction, the growth patterns are the islands of grain structures and the contribution of impingement becomes important. Grain boundary scattering will dominate the later stages.

The experimental results show that it is possible to distinguish the differences between the nucleation kinetics, nucleation densities, and nuclei distributions from the scattering curves, when the transformed fraction is low. Experimental data confirm Porod's law, that is, the q^{-4} dependence of the tails. This indicates that the final slope of the structure function is proportional to q^{-4}, since the real-space structure contains a well-defined interface between the spherulitic growth domains.

Assuming spherulitic domains with a size distribution and no interference between the spherulitic domains before impingement, a scaling relation of the structure function is found experimentally for the free growth of domains during the postnucleation stage. The scaling is the system dynamic behavior and demonstrates that spherulitic domains grow in size linearly with time. The scaling is valid for times long enough that the influence of the initial conditions has decayed; i.e., the nucleation event is not dominant. However, the scaling will break down when some impinged spherulitic domain clusters become time-independent.

Acknowledgment. The authors appreciate Dr. Tomohiro Tsuji for valuable discussion. T.H. would like to thank Dr. Hajim Tanaka for technique instruction on 2DFFT.

References and Notes

(1) Thomas, E. L. Structure and Properties of Polymers. In *Materials Science and Technology*; Cahn, R. W., Haasen, P., Kramer, E. J., Eds.; VCH: Weinheim, 1993; Vol. 12.

(2) Keith, H. D.; Padden, F. J., Jr. *J. Appl. Phys.* **1963**, *34*, 2409. *Crystallization of Polymers*; NATO ASI Series; Kluwer Academic Publishers: Dordrecht, 1993. Huang, T.; Rey, A. D.; Kamal, M. R. *Polymer* **1994**, *25*, 5434.

(3) *Solidification Processes in Polymers*; Gedde, U., Jansson, J. F., Eds.; Springer-Verlag: New York, 1992.

(4) Gunton, J. D.; San Miguel, M.; Sahni, P. In *Phase Transitions and Critical Phenomena*; Domb, C., Lebowitz, J. L., Eds.; Academic Press: London, 1983; Vol. 8, p 267. Gunton, J. D.; Droz, M. *Introduction to the Theory of Metastable and Unstable States*; Springer-Verlag: Berlin, 1983.

(5) Kolmogorov, A. N. *Izv. Akad. Nauk SSSR, Ser. Matem No.* **1937**, *3*, 355−359. Johnson, W.; Mehl, R. F. *TAIME* **1939**, *135*, 416. Avrami, M. *J. Chem. Phys.* **1939**, *7*, 1103, 212, 177.

(6) Sekimoto, K. *Phys. Lett. A* **1984**, *105*, 390; *J. Phys. Soc. Jpn.* **1984**, *53*, 2425; *Physica A* **1986**, *137*, 96.

(7) Axe, J. D.; Yamada, Y. *Phys. Rev. B* **1986**, *34*, 1599.

(8) Ohta, S.; Ohta, T.; Kawasaki, K. *Physica A* **1987**, *140*, 478.

(9) Hermann, H. In *Stochastic Models of Heterogeneous Materials, Materials Science Forum*; Murch, G. E., Wohlbier, F. H., Eds.; Trans. Technol. Publications: Zurich, 1991; Vol. 78. Uebele, P.; Hermann, H. *Model. Sim. Mater. Sci. Eng.* **1996**, *4*, 203.

(10) Stein, R. S.; Srinivasarao, M. *J. Polym. Sci. Part B: Polym. Phys.* **1993**, *31*, 2003 and references therein.

(11) Prud'homme, R. E.; Stein, R. S. *Macromolecules* **1971**, *4*, 668. Hashimoto, T.; Prud'homme, R. E.; Stein, R. S. *J. Polym. Sci. Part B: Polym. Phys.* **1973**, *11*, 709.

(12) Okada, T.; Saito, H.; Inoue, T. *Macromolecules* **1992**, *25*, 1908. Lee, C. H.; Saito, H.; Inoue, T. *Macromolecules* **1993**, *26*, 6566.

(13) Krishnamurti, S.; Goldburg, W. I. *Phys. Rev. A* **1980**, *22*, 2147. Cumming, A.; Wiltzius, P.; Bates, F. S.; Rosedale, J. H. *Phys. Rev. A* **1992**, *45*, 885. Schatzel, K.; Ackerson, B. J. *Phys. Rev. E* **1993**, *48*, 3776. Balsara, N. P.; Chenchy Lin Hammouda, B. *Phys. Rev. Lett.* **1996**, *77*, 3847.

(14) Tanaka, H.; Hayashi, T.; Nishi, T. *J. Appl. Phys.* **1986**, *59*, 3627.

(15) Guinier, A.; Fournet, G. *Small Angle Scattering of X-rays*; Wiley: New York, 1955. Glatter, O.; Kratky, O. *Small-Angle X-ray Scattering*; Academic Press: New York, 1982.

(16) Porod, G. In *Small-Angle X-ray Scattering*; Glatter, O., Kratky, O., Eds.; Academic Press: New York, 1982.

(17) Huang, T.; Tsuji, T.; Rey, A. D.; Kamal, M. R. *Phys. Rev. E* **1998**, *58*, No. 5, in press.

(18) Kotlarchyk, M.; Chen, S.-H. *J. Chem. Phys.* **1983**, *79*, 2461.

(19) Huang, T. Ph.D. Thesis, McGill University, 1997.

(20) Billotet, C.; Binder, K. *Z. Phys.* **1979**, *B32*, 195. Ohta, T.; Jasnow, D.; Kawasaki, K. *Phys. Rev. Lett.* **1982**, *49*, 11233.

(21) Bray, A. J. *Adv. Phys.* **1994**, *43*, 357 and references therein.

(22) Lifshitz, I. M.; Slyozov, V. V. *J. Phys. Chem. Solids* **1961**, *19*, 35.

(23) Imai, M.; Kaji, K.; Kanaya, T.; Sakai, Y. *Phys. Rev.* **1995**, *B52*, 12696. Fukao, K.; Miyamoto, Y. *Phys. Rev. Lett.* **1997**, *79*, 4613.

(24) Tashiro, K.; Imanishi, K.; Izumi, Y.; Kobyashi, M.; Kobyashi, K.; Satoh, M.; Stein, R. S. *Macromolecules* **1995**, *28*, 8477.

(25) Huang, T.; Tsuji, T.; Kamal, M. R.; Rey, A. D. *Phys. Rev. E* **1998**, *58*, 789.

MA9801218